Effect of soot microstructure on its ozonization reactivity

Chong Han, Yongchun Liu, Jinzhu Ma, and Hong He

Additional information on J. Chem. Phys.
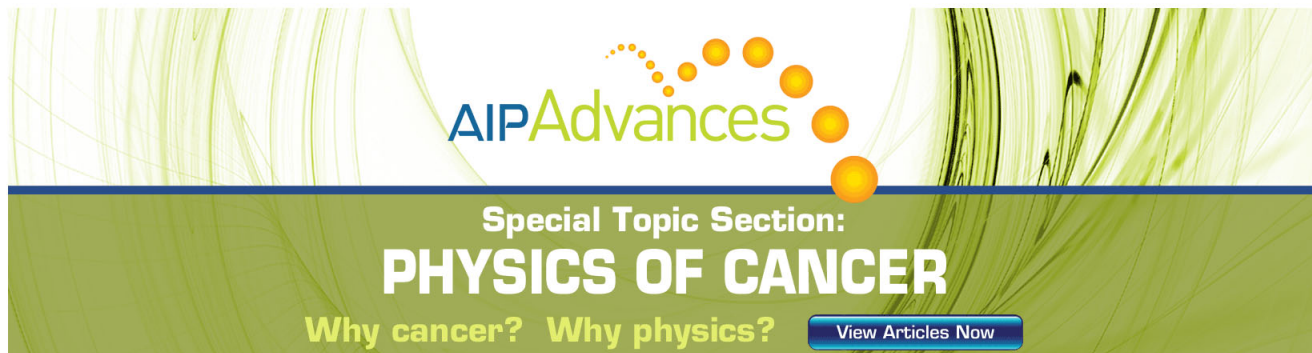
Effect of soot microstructure on its ozonization reactivity

Chong Han, Yongchun Liu, Jinzhu Ma, and Hong He[a)]
Research Center for Eco-Environmental Sciences, Chinese Academy of Sciences, Beijing 100085, China

Large uncertainty among the measured uptake coefficients of O_3 on soot highlights the importance of the sources and chemical structures of soot samples in this reaction. Soot samples with different microstructures were prepared by combusting *n*-hexane under controlled conditions. Their reactivities to O_3 were further investigated using *in situ* Raman spectroscopy. The fuel/oxygen ratio in the combustion experiments not only affected the diameter of the primary particles, but also influenced the micro-chemical structure of soot. Average diameters of soot particles decreased with the decreasing fuel/oxygen ratio. Compared to the "fuel-rich" flame soot, the "fuel-lean" flame soot showed lower structural uniformity with higher disordered carbon content at the graphene layer edges (*D1* band) and the surface graphene layers (*D2* band) and the amorphous carbon content (*D3* band). This disordered carbon was identified as the reactive component for the ozonization of both the "fuel-rich" and "fuel-lean" flame soot samples. The kinetics study demonstrated that the disordered carbon at the surface graphene layers was more active than that at the graphene layer edges in one sample, and the reactivity of these two microstructures types to O_3 in the "fuel-rich" flame soot was higher than that in the "fuel-lean" flame soot. © *2012 American Institute of Physics.* [http://dx.doi.org/10.1063/1.4747190]

I. INTRODUCTION

Soot particles, formed by incomplete combustion of fossil and biomass fuels, are ubiquitous in the atmosphere. They play a significant role in the radiative budget of the atmosphere and climate change,[1,2] and also pose a health risk to humans due to their possible carcinogenic and mutagenic bound compounds.[3] The climatic and toxic effects of soot, however, greatly depend on their composition and microstructure, which are significantly affected by the sources, combustion conditions, and atmospheric processing. In particular, the heterogeneous reaction processes of soot have attracted intense attention[4–6] since these processes not only affect the sources and sinks of some important gas-phase species such as HONO and O_3,[7–12] but also lead to changes in morphological, hygroscopic, and optical properties of soot aggregates.[4,13,14]

Up to now, reaction kinetics have been mainly concerned with the heterogeneous reactions of trace gases, including NO_2, HNO_3, O_3, and H_2SO_4, on different soot samples.[9,12,15,16] Soot also can provide adsorption sites of H_2O,[17–19] serving as cloud concentration nuclei (CCN) and ice nuclei (IN). However, the reactivity for a given reaction system shows great difference.[7,8,20] For example, the uptake coefficients of NO_2 on different kinds of soot varies from 10^{-1} to 10^{-8}. Over the past several decades, the heterogeneous reaction of soot with O_3 has attracted more and more attention due to its potential contribution to chemical transformation of O_3 in the upper troposphere and low stratosphere.[21,22] Previous studies also have investigated the uptake coefficients of O_3 on various soot samples such as flame soot,[23] spark

discharge soot,[24] and commercially available soot.[25] However, the uptake coefficients of O_3 on soot are highly variable and varies from 10^{-3} to 10^{-8}. This significant variance may be dependent on the source of carbon, soot surface area, soot porosity, experimental system, and concentration of reactants, relative humidity, and surface coverage.[26] Such great variability can contribute to the uncertainty of whether or not soot aerosols play an important role in chemical transformation of O_3. These controversial results also imply that the structure of soot may be a crucial factor for the differences in reactivity of soot with O_3. At present, however, little is known about the structure-activity relationship for the reaction of soot during heterogeneous reaction with O_3.

In general, soot particles consist of both graphitic and amorphous domains.[27] The graphite-like domains, which are randomly oriented and connected to one another by single planes or by amorphous carbon,[27] are primarily composed of three to four turbostratically stacked graphene layers.[28] The amorphous domains are disordered mixtures, including polycyclic aromatic hydrocarbons and other organic and inorganic components.[28,29] Functional groups including carboxylic acid, lactone, carboxylic anhydride, phenol, carbonyl, ether, and quinine are well identified on soot surfaces.[30] In our previous work, we found that different soot microstructures showed different reactivities to O_3 at room temperature, even within one soot sample.[4] This has also been observed for soot oxidation by O_2 at high temperature.[31] Both the origin and formation conditions significantly influence the structure of soot. Additionally, the interaction between soot and O_3 may not only lead to stratospheric ozone consumption but also cause enhancement of CCN and IN activity of soot in the troposphere.[4,12,32] In the present study, therefore, soot samples with different microstructural features were obtained

a)Author to whom correspondence should be addressed. Electronic mail: honghe@rcees.ac.cn. Tel.: +86-10-6284-9123. Fax: +86-10-6292-3563.

under well-controlled combustion conditions, and their reactivities to O_3 were investigated using *in situ* Raman spectroscopy. The results will help to understand the essence of variance in reactivity of soot with important trace gases.

II. EXPERIMENTAL

Soot was produced using a co-flow home-made burner system as described in previous papers.[33, 34] The co-flow burner consisted of a diffusion flame maintained in a flow of synthetic air, which was controlled by mass flow meters to regulate the fuel/oxygen ratio. The fuel was fed by a cotton wick extending into the liquid fuel reservoir. Soot was collected on aluminum foil over the diffusion flame. The molar ratio of fuel (measured by the consumed *n*-hexane mass) to oxygen (obtained by the entrained air flow volume) during the combustion process was in the range of 0.100–0.200. We used *n*-hexane (AR, Sinopharm Chemical Reagent Lo., Ltd.) as the fuel. Soot particles were collected about 4 cm over the flame.

The particle sizes of soot were examined using a transmission electron microscope (H-7500, Hitachi). Soot produced in *n*-hexane flame was directly deposited on a Cu microgrid. The acceleration voltage was set to 200 kV for measurements. ImageJ 1.41 software was used to analyze the diameter of soot particles. The specific surface area of soot was measured by nitrogen Brunauer-Emmett-Teller physisorption (Quantachrome Autosorb-1-C).

In situ Raman spectra for the reaction of soot with O_3 were recorded on a UV resonance Raman spectrometer (UVR DLPC-DL-03). A continuous diode pumped solid state laser beam (532 nm) was used as the exciting radiation, and a source power with 40 mW was used. The diameter of the laser spot on the sample surface was focused at 25 μm. The spectra resolution was 2.0 cm^{-1} and exposure time for each scan was 50 s. During reaction with O_3, soot samples were exposed to the laser only when each scan was performed. Thus, the total exposure time was less than 20 min in the experiment. As shown in Fig. S1 of the supplementary material,[41] no sample modification was observed when the sample was continuously irradiated for 60 min in air under the experimental conditions. This demonstrates that the laser has no effect on changes of soot samples.

Soot particles were deposited on aluminum-foil and placed in a steel sample holder. The sample in the *in situ* reactor was purged with 100 mL min^{-1} of simulated air (80% high purity N_2 and 20% high purity O_2) for 30 min at 298 K. Then, 80 ppm O_3 in 100 mL min^{-1} air was introduced into the reactor and *in situ* Raman spectra were recorded under atmospheric pressure. The O_3 was generated by irradiation mixture flow of high purity O_2 and N_2 using a mercury lamp with wavelength of 185 and 254 nm. The concentration of O_3 was measured by an ozone monitor (Model 202, 2B Technology). The temperature was held at 298 K during the reaction.

The functional groups of the soot samples were also characterized using a NEXUS 6700 (Thermo Nicolet Instrument Corp.) Fourier transform infrared spectrometer equipped with a high-sensitivity mercury-cadmium-telluride detector cooled by liquid N_2 and an attenuated total internal reflection infrared

(ATR-IR) cell. Soot particles from the *n*-hexane flame were directly deposited on the ZnSe crystal in ATR-IR cell. Then, *in situ* spectra of soot during reaction with O_3 were recorded (100 scans, 4 cm^{-1} resolution) using the blank ZnSe as reference. The reaction conditions in the ATR-IR experiment were the same as that in the Raman experiment.

Spectra of the soot samples were recorded over the range of 800–2000 cm^{-1} and data fitting was performed using PeakFit software to determine spectral parameters. Usually, four Lorentzian-shaped bands (*D1*, *D2*, *D4*, and *G*, centered at about 1360, 1620, 1180, 1580 cm^{-1}, respectively) and one Gaussian-shaped band (*D3*, centered at around 1500 cm^{-1}) are identified by curve fitting in the first-order Raman spectra.[4, 28, 31] Each band in Raman spectroscopy can be assigned to a class of structures and compositions in soot. Functional groups such as C–C, C=C, and C=O, can be assigned to different bands. The *D1* band arises from the A_{1g} symmetry mode of the disordered graphitic lattice located at the graphene layer edges. The *D2* band is attributed to the E_{2g} symmetry stretching mode of the disordered graphitic lattice located at the surface graphene layers. The *D3* band originates from the amorphous carbon fraction of soot. The *D4* band is related to the A_{1g} symmetry mode of the disordered graphitic lattice or C–C and C=C stretching vibrations of polyene-like structures. The *G* band is assigned to the ideal graphitic lattice with E_{2g} symmetry vibration mode. Additionally, functional group C=O in ketone, lactone, and anhydride species, can contribute to band at 1750 cm^{-1} according to our previous work.[4] Therefore, we also performed curve fitting with the same procedure as mentioned above.

III. RESULTS AND DISCUSSION

A. Structural features of soot samples produced at different fuel/oxygen ratios

The changes in average diameter (*d*) and specific surface area (*S*) of soot samples are summarized in Table I. Average diameter of soot particles decreased from (29.8 ± 8.1) nm to (23.4 ± 7.6) nm as the fuel/oxygen ratio decreased from 0.193 to 0.109. The decrease amplitude in average diameter was about 18.9%. The specific surface area was in the range of (52.0–56.0) m^2 g^{-1} with the fuel/oxygen ratio changing. These values were close to that of *n*-hexane soot measured by Choi and Leu.[35]

Figure 1 shows the first-order Raman spectra in the range of 800–2000 cm^{-1} of soot samples produced at different fuel/oxygen ratios, and displays the well-known bands of soot

TABLE I. Average diameters and specific surface areas of soot obtained at different fuel/oxygen ratios.

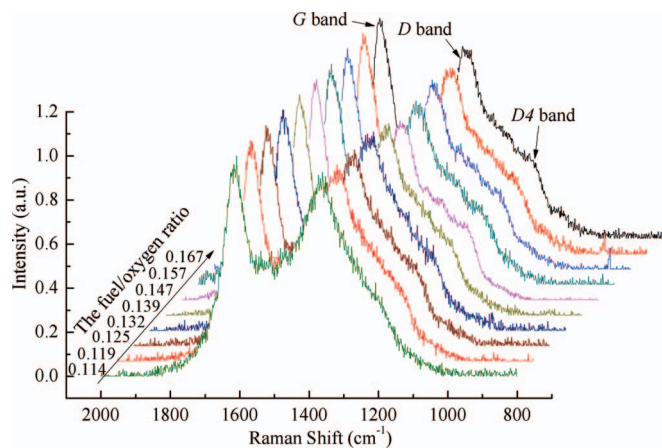| Fuel/oxygen ratio	Average diameter (nm)	Specific surface area (m^2 g^{-1})
0.193	29.8 ± 8.1	52.1
0.147	26.5 ± 7.2	55.7
0.125	24.4 ± 7.8	52.9
0.109	23.4 ± 7.6	53.6

FIG. 1. Raman spectra in the range of 800–2000 cm^{-1} of fresh flame soot produced at different fuel/oxygen ratios.
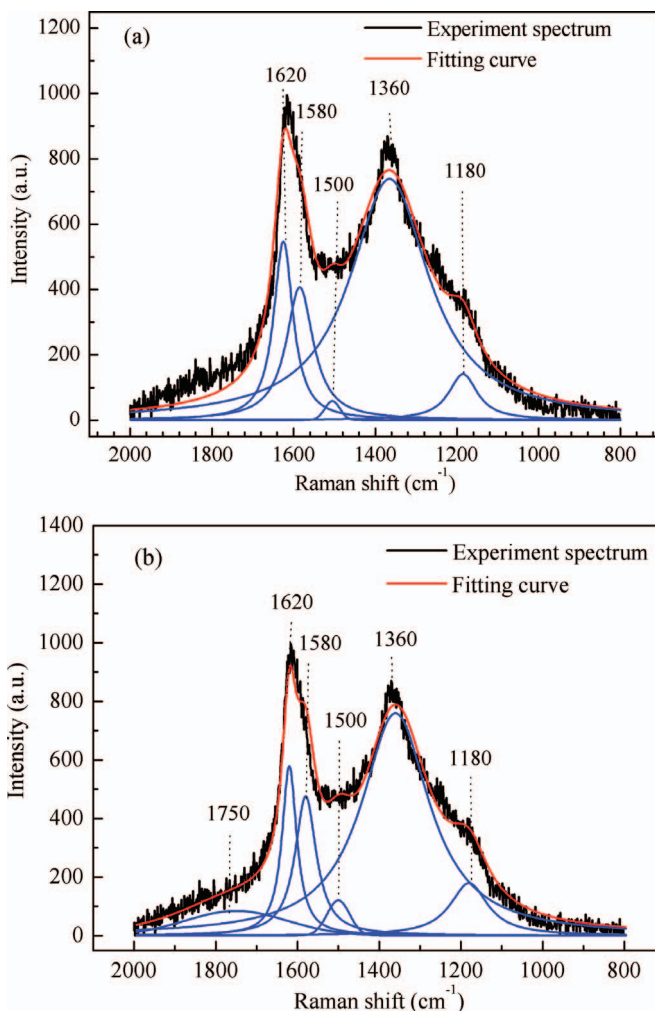

FIG. 2. Curve fitting results for fresh soot with the fuel/oxygen ratio of 0.147. (a) and (b) are curve fitting results of Raman spectra based on five and six bands, respectively.

near 1580 cm^{-1} (*G* band) and 1360 cm^{-1} (*D* band). The *G* band corresponding to the E_{2g} symmetry of an ideal graphitic lattice is a typical characteristic of natural graphitic crystals. The *D* band assigned to the A_{1g} symmetry mode is only observed for disordered graphite. As seen in Fig. 1, the Raman spectra of these samples were very similar. The intensity of the shoulder peak (*D4* band, around at 1180 cm^{-1}) of the *D* band, however, decreased obviously with the decrease in fuel/oxygen ratio. This might be partially related to the low content of the disordered carbon at the graphene layer edges or polyene-like component in soot obtained under low fuel/oxygen ratio.

To quantitatively analyze the microstructure features of these samples, curve fitting was performed in light of the procedure introduced in Sec. II. The results of soot produced at the fuel/oxygen ratio of 0.147 are illustrated in Fig. 2. Although the main body of the fitting spectrum was in good agreement with the experimental spectrum in Fig. 2(a), a large residual at around 1750 cm^{-1} was observed. The recorded value (black line) was obviously higher than the analyzed results in the ranges, suggesting that some surface species formed in the combustion of *n*-hexane may contribute to the Raman scattering in this region. In our previous work, we also observed a similar phenomenon for ozone oxidized Printex U soot sample and ascribed this to the formation of surface carbonyl groups including ketone, lactone, and anhydride species.[4] These species have also been observed in kerosene soot.[13] Thus, we postulate that these groups may be formed during the combustion of *n*-hexane. To confirm this assumption, fresh soot deposited on the ZnSe crystal was enough to obtain good IR spectra. A broad band in the range of 1780–1680 cm^{-1} can be seen in Fig. 3. The curve fitting results with three Gaussian bands at 1760 cm^{-1} ($v_{C=O}$ in anhydride), 1750 cm^{-1} ($v_{C=O}$ in lactone), and 1730 cm^{-1} ($v_{C=O}$ in ketone),[13] coincided well with the experimental spectrum. Therefore, a Gaussian band at 1750 cm^{-1} was considered in the curve fitting procedure of the Raman spectra. Figure 2(b) shows the curve fitting results with six bands, which exhibited better consistency with the observed spectrum. The correlation coefficient was greater than 0.990. Particularly, the observed spectrum (black line) coincided well with the

fitted curve (red line) in the region around 1750 cm^{-1}. As shown in Fig. S2 of the supplementary material,[41] Raman spectra also exhibited broad signals in the range of 2500–3500 cm^{-1}, while the intensity of which is rather lower than that in the range of 800–2000 cm^{-1}. This also has been found in previous paper.[28] Analysis of bands in the range of 2500–3500 cm^{-1} was performed in Fig. S2 of the supplementary material.[41] Because signal of Raman spectra in the range of 2500–3500 cm^{-1} is weak and can be ascribed to overtones and combination of Raman spectra in the range of 800–2000 cm^{-1}, we would focus on changes in Raman spectra in the range of 800–2000 cm^{-1}.

Figure 4(a) shows the changes in the full widths at half maximum (FWHMs) for the six bands in Fig. 2(b) when the fuel/oxygen ratio decreased from 0.193 to 0.109. We compared results of three analyses of separate samples produced at the same fuel/oxygen ratio, difference of which was negligible due to good reproducibility. The error bars demonstrate the standard deviations of three independent fitting results for one spectrum, reflecting variance for every independent curve fitting result by PeakFit software. For the *D1*, *D2*, *D3*, and *G* bands, the FWHMs showed a pronounced
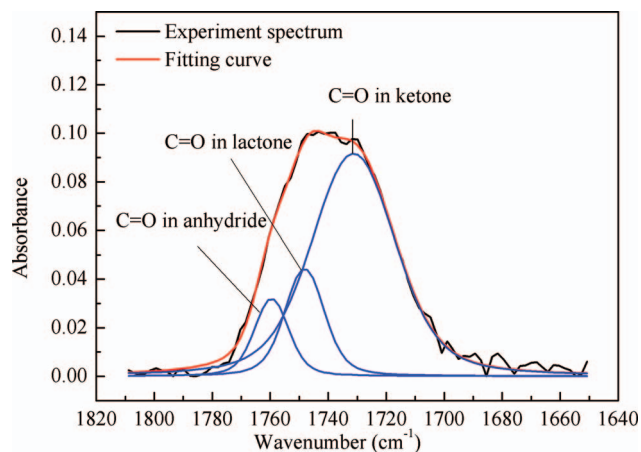
FIG. 3. Curve fitting results of ATR-IR spectra based on three bands for fresh soot with the fuel/oxygen ratio of 0.147.

increase as the fuel/oxygen ratio decreased. Compared to the FWHMs of the *D1*, *D2*, *D3*, and *G* bands for the soot sample produced at 0.193 of the fuel/oxygen ratio, the FWHMs of these four bands for the soot sample produced at 0.109 of the fuel/oxygen ratio increased by 21.1, 16.4, 26.4, and 10.3 cm^{-1}, respectively. The increase in FWHM indicated an increase in the degree of disorder for this kind of soot microstructure.[28,31] These results suggest that the chemical heterogeneity of the disordered carbon at the graphene layer edges (*D1*) and the surface graphene layers (*D2*), amorphous carbon (*D3*), and ideal graphitic lattice (*G*), increased as the fuel/oxygen ratio decreased. However, the FWHM of the *D4* band decreased by 11.8 cm^{-1}, which implies that the degree of disorder of the disordered graphitic lattice or polyene-like structures decreased with decreasing the fuel/oxygen ratio. The change in the FWHM of the band at 1750 cm^{-1} (ketone, lactone, and anhydride species) was complicated. When the fuel/oxygen ratio was larger than 0.147, the FWHM of the

band at 1750 cm^{-1} increased with decreasing the fuel/oxygen ratio; it then began to decrease when the fuel/oxygen ratio was lower than 0.139.

Figure 4(b) shows the changes in relative content of the six bands. Compared to the integrated areas of the *D1*, *D2*, and *D3* bands for the soot sample produced at 0.193 of the fuel/oxygen ratio, the integrated areas of these three bands for the soot sample obtained at 0.109 of the fuel/oxygen ratio increased by 5.1%, 3.8%, and 1.5%, respectively. These results indicate that the disordered carbon at the graphene layer edges and surface graphene layers as well as amorphous carbon were more easily formed under low fuel/oxygen ratios. However, the integrated areas of the *D4* and *G* bands decreased by 4.5% and 3.6%, respectively. This confirmed that the disordered graphitic lattice or polyene-like structures and ideal graphitic lattice had a relatively low content in soot obtained under low fuel/oxygen ratios. Similar to the FWHM change for the band at 1750 cm^{-1}, its integrated area had a knee point around (0.147–0.139) of the fuel/oxygen ratio, which implies that an appropriate fuel/oxygen ratio existed for the formation of ketone, lactone, and anhydride species during combustion of *n*-hexane. Based on these results, we concluded that the fuel/oxygen ratio had an impact on the microstructure of soot formed by fuel combustion.

B. Reactivities to O₃ for soot with different microstructure

In our previous work,[4] we only investigated the structural and hygroscopic changes of a model soot (Printex U) during a heterogeneous reaction with O_3, while how soot microstructures influence its ozonization reactivity is not clear. In the present work, we focused on the effect of soot microstructure on its ozonization reactivity. Soot samples with different microstructures were prepared under well-controlled
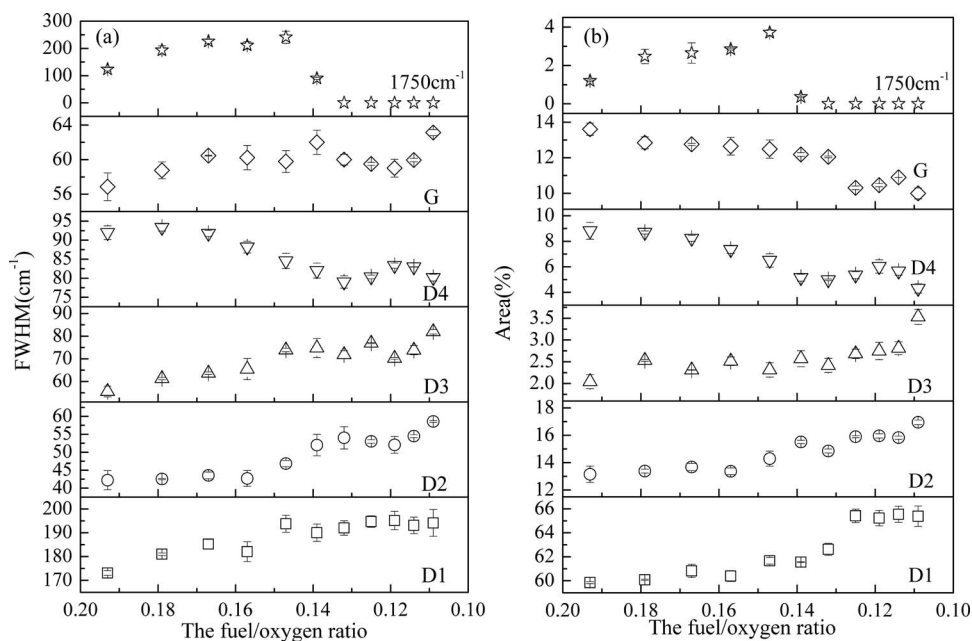

FIG. 4. Summaries of (a) FWHM and (b) percentage of integrated area of each band for fresh soot prepared under different fuel/oxygen ratios.
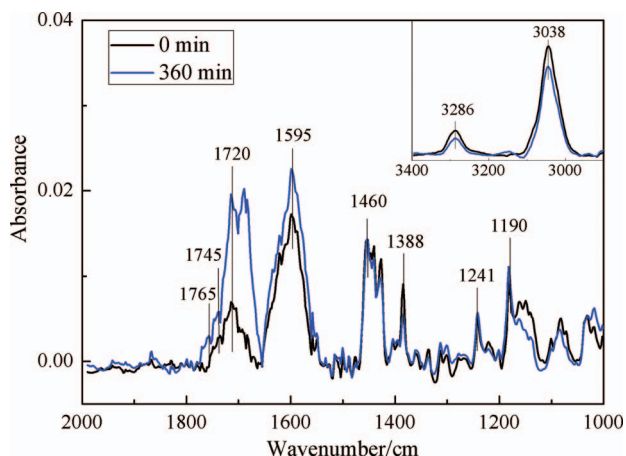
FIG. 5. Changes of ATR-IR spectra in the range of 1000–2000 cm^{-1} of "fuel-rich" flame soot in 80 ppm O$_3$ for 360 min at 298 K.

FIG. 6. *In situ* Raman spectra of the "fuel-rich" flame soot in the range of 800–2000 cm^{-1} during the reaction with 80 ppm O$_3$ at 298 K under atmospheric pressure.

combustion conditions. In Fig. 4, fuel/oxygen ratio has been linked to the changes in microstructures. Here, the two soot samples with significantly different microstructures were selected to study the role of soot microstructure in the reaction with O$_3$. One was produced in a "fuel-rich" flame at a relatively high fuel/oxygen ratio (0.193), and the other was generated in a "fuel-lean" flame at a relatively low fuel/oxygen ratio (0.147). As discussed above, the soot samples had different microstructures. Compared to the soot produced in "fuel-rich" flame, the soot produced in "fuel-lean" flame had higher structural heterogeneity and content for the disordered carbon at the graphene layer edges and surface graphene layers, amorphous carbon, and ketone, lactone, and anhydride species. However, the disordered graphitic lattice or polyene-like structures in the "fuel-lean" flame soot showed lower structural heterogeneity and content. In addition, relatively low structural uniformity and content of ideal graphitic lattice in the "fuel-lean" flame soot was also observed.

Figure 5 shows changes of IR spectra in the range of 1000–2000 cm^{-1} of soot after being oxidized by 80 ppm O$_3$ for 360 min. Content of soot deposited on the ZnSe crystal was small to reduce limitation of O$_3$ diffusion, leading to difference in intensity between Figs. 3 and 5. A significant increase in intensity of IR spectra in the range of 1650–1800 cm^{-1} indicates formation of ketone ($v_{C=O}$, 1720 cm^{-1}), lactone ($v_{C=O}$, 1745 cm^{-1}), and anhydride species ($v_{C=O}$, 1765 cm^{-1}).[4,13] However, changes of the corresponding bands of v_{C-O} groups in lactone and anhydride species in the range of 1000–1300 cm^{-1} were not observed due to its weak infrared absorption and the small amount of lactone and anhydride formed on soot. The peak at 1595 cm^{-1}, which can be ascribed to carbonyl groups conjugated to aromatic ring, also showed an increase after 360 min. Previous studies also observed formation of these species in reaction of soot with O$_3$.[13] At the same time, intensities of peak at 3038 cm^{-1} assigned to aromatic C–H and peak at 3286 cm^{-1} related to alkyne ($\equiv$C–H) decreased.

Figure 6 shows the *in situ* Raman spectra for ozonation of the "fuel-rich" flame soot. The concentration of O$_3$ was 80 ppm. As shown in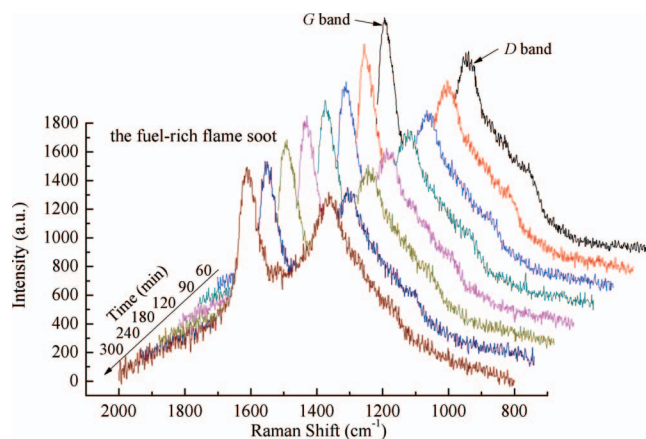 Fig. 6, the signal intensities of the D and G bands decreased slightly with reaction time due to the consumption of these micro domains during reaction with O$_3$. This was also observed for the ozonation of the "fuel-lean" flame soot. Previous studies have identified the decomposition of soot by O$_3$.[36] In our previous work,[4] however, an opposite phenomenon was observed for the ozonation of commercial soot (Printex U) at the beginning of reaction. The increase in spectra intensity was ascribed to the removal of surface organic impurities, which led to fluorescence interference, by purging with simulated air or being oxidized by O$_3$. Soot with a large specific surface area can react with active constituents and adsorb some organic species in the atmosphere.[5–8,13] It should be pointed out that the soot sample used in this study may have less surface organic impurities than that bound to Printex U, because the former was fresh soot, while the latter had been stored in air for a long time. Once the impurities were fully removed, intensity of D and G band in Raman spectra of Printex U would also decrease. Thus, consumption of soot in the reaction should contribute to a decrease in intensity of D and G bands.

As discussed in Fig. 3, surface carbonyl compounds were observed in the soot samples. IR spectra also confirmed the formation of these species during reaction with O$_3$ (Fig. 5). This can cause a larger residual in the region around 1750 cm^{-1} [Fig. S3(a) of the supplementary material[41]]. In our previous work,[4] another band at 1060 cm^{-1} for the ozonized Printex U by O$_3$ was also considered because of the existing residual around 1060 cm^{-1}. However, the residual around 1060 cm^{-1} was not observed in this case, which may be due to different origins of soot [Fig. S3(a) of the supplementary material[41]]. Therefore, the *in situ* Raman spectra were also analyzed with the *D1*, *D2*, *D3*, *D4*, *G*, and 1750 cm^{-1} bands [Fig. S3(b) of the supplementary material[41]]. Figure 7 summaries the changes in the FWHM for each band as a function of reaction time. After reacting for 360 min, the FWHM of *D1*, *D2*, *D3*, *D4*, *G*, and 1750 cm^{-1} for the "fuel-rich" flame soot [Fig. 7(a)] increased by 36.0, 5.9, 10.7, 88.8, 6.1, and 133.9 cm^{-1}, respectively. The pronounced increase in the FWHMs for all bands suggests that the heterogeneous reaction of soot with O$_3$ led to a decrease
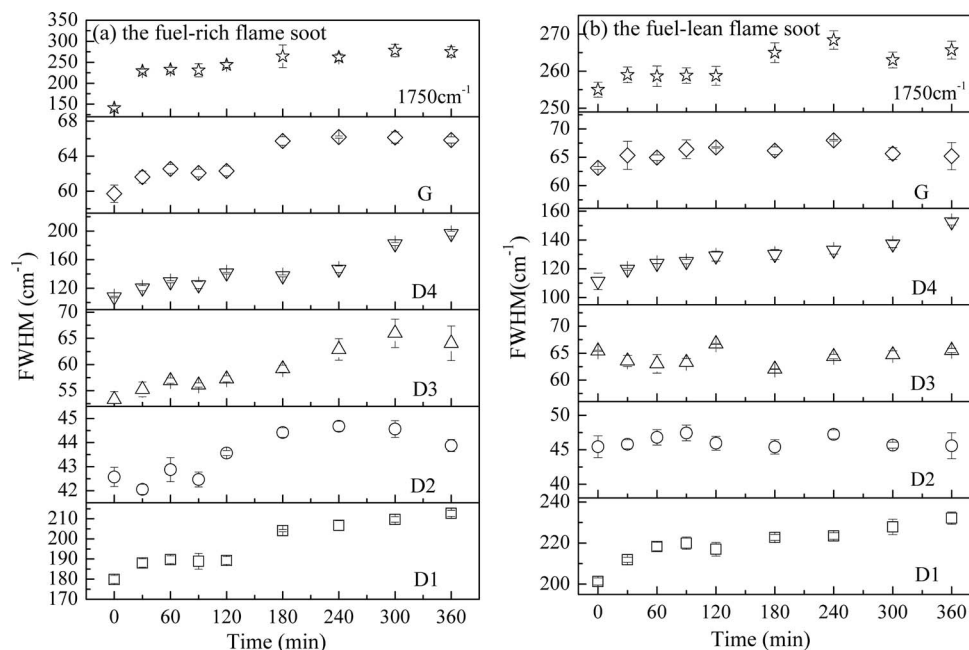
FIG. 7. Temporal changes of FWHM for each band in the "fuel-rich" flame soot (a) and "fuel-lean" flame soot (b) during the reaction with 80 ppm O_3 at 298 K under atmospheric pressure.

in the degree of structural order of all regions in soot. It should be pointed out that if newly formed species as shown at 1595 cm^{-1} in IR spectra also have Raman signal, these species may partially attribute to broader FWHMs of *D2* and *G* bands. For "fuel-lean" flame soot [Fig. 7(b)], however, the FWHM of only three bands (*D1*, *D4*, and 1750 cm^{-1} band) increased by 30.9, 41.4, and 10.7 cm^{-1}, respectively. The increasing amplitude for the FWHM of each band for the "fuel-lean" flame soot was also smaller than that for the "fuel-rich" flame soot. These results imply that the uniformity for the disordered carbon at the graphene layer edges, disturbed graphitic lattice, ketone, lactone, and anhydride species exhibited a pronounced decrease. The FWHM of *D2*, *D3*, and *G* bands remained almost unchanged, indicating a near-constant degree of structural order of the disordered carbon at the surface graphene layers, amorphous carbon, and the ideal graphitic lattice. Although Raman spectroscopy has become an efficient tool for investigation of soot microstructure,[27,28,31] it should be pointed out that the limited ability of Raman spectroscopy to resolve disorder also may be one reason why the FWHM of *G*, *D2*, and *D3* bands in the "fuel-lean" flame soot remained almost unchanged. In other words, if the new peaks formed in reaction have the similar chemical disorder degree and has the same vibrational frequencies with the *G*, *D2*, and *D3* bands, it may also lead to the absence in the net change in the peak widths.

During the oxidation process of GFG soot with O_2 at 523 and 573 K, a decrease in the FWHMs for all bands with reaction time was observed in previous research,[31] which indicates that the reaction of GFG soot with O_2 at high temperature increased the structural order degree. The opposite trend may be related to different reaction conditions. According to Dippel and Gruber,[27,37] for heat treated soot and black carbon, less-graphitized carbon will likely be transformed into

graphitic carbon. Additionally, because volatile organic carbonaceous materials adsorbed on soot or newly formed by oxidation, which may contribute to the low degree of structural order in soot, are not strongly bonded to the graphitic domains, they easily desorb from the surface of soot when purged by air flow at high temperature. Therefore, reaction conditions may play an important role in the changes of the structural order of soot.

Figure 8(a) shows the change in the percentage of integrated area for each band in the "fuel-rich" flame soot during reaction with O_3. Upon ozonation, the integrated areas of the *D1* and *D2* bands showed a decrease. After reacting for 360 min, the integrated areas decreased by 3.5% and 4.8% for *D1* and *D2* bands, respectively. In IR spectra, increase in intensity of the peak at 1595 cm^{-1} was ascribed to formation of carbonyl groups conjugated to aromatic ring. These species may also give Raman signal, thus having a negative effect on decrease in integrated area of *D2* band. Thus, integrated area of *D2* band may actually show lager decrease amplitude. This implies that the disordered carbon at the graphene layer edges and surface graphene layers was consumed during reaction with O_3. The integrated areas of *D3*, *D4*, and *G* bands remained unchanged, indicating that the heterogeneous reaction had little effect on the amorphous carbon, disordered graphitic lattice, and ideal graphitic lattice. However, the integrated area of band at 1750 cm^{-1} increased by 8.8%, suggesting the formation of ketone, lactone, and anhydride species during this reaction. These results also indicate that different regions in soot have different reactivity to O_3. As shown in Fig. 8(b), similar to that for the "fuel-rich" flame soot, the integrated area of each band in the "fuel-lean" flame soot also showed the same change trend. However, the degrees of decrease for *D1* and *D2* bands and the increase for band at 1750 cm^{-1} were less than that of the "fuel-rich" flame soot. This implies
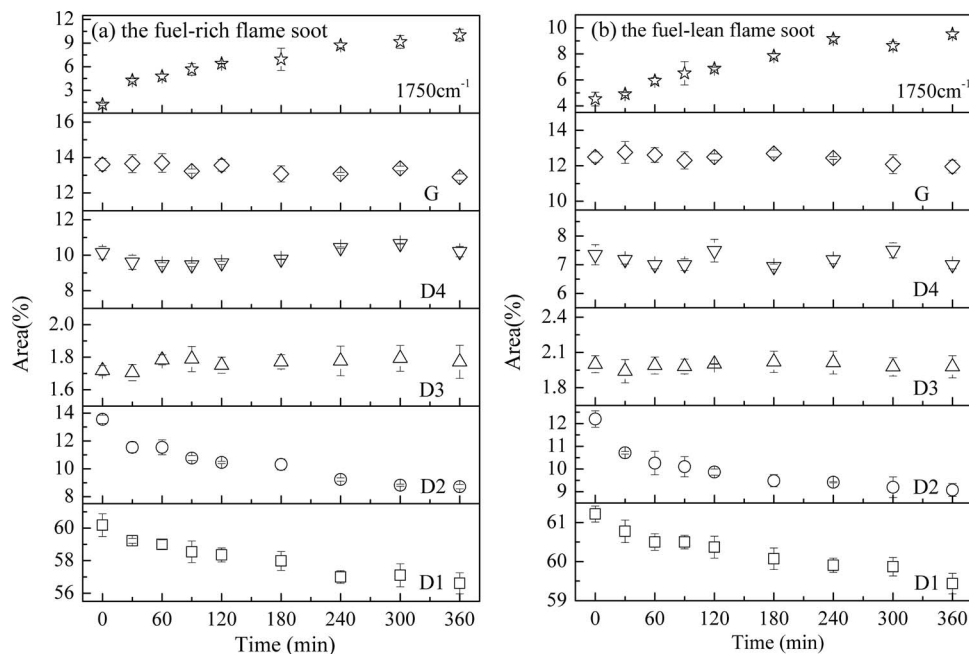
FIG. 8. Temporal changes in integrated area percentage of each band for the "fuel-rich" (a) and the "fuel-lean" (b) flame soot during the reaction with 80 ppm O_3 at 298 K under atmospheric pressure.

that the "fuel-rich" and "fuel-lean" flame soot samples had the same active sites and the same products for ozonation. However, the relative content of the consumed disordered carbon at the graphene layer edges and surface graphene layers in the "fuel-lean" flame soot was lower than that in the "fuel-rich" flame soot, which indicates that the two samples had different reaction kinetics.

As for the oxidation process of Printex U with O_3,[4] we observed a decrease in the integrated area of *D3*, suggesting the consumption of amorphous carbon during reaction. After being ozonised for 4 h, content of amorphous carbon decreased to about 2.0% and almost remained unchanged at this value with increasing ozonation time. It means that some amorphous carbon which were not accessible to O_3 and therefore did not participate in the reaction. This study revealed, however, that it was difficult for amorphous carbon of *n*-hexane soot to react with O_3. It was found that the content of amorphous carbon in *n*-hexane soot is in the range of 2.0%–2.5% approaching to that in Printex U soot sample ozonized for 4 h by O_3. One possible reason is that high active amorphous carbon may be consumed during production process of soot by combusting *n*-hexane. Another possible reason is that content of amorphous carbon, most of which may be located at inner layers, may be rather lower at surface layers on soot. A poor diffusion of O_3 through surface layers may limit the consumption of amorphous carbon. The difference in the activities of the *D1* and *D4* bands in the *n*-hexane soot (this work) and Printex U might originate from the different soot sources. These results demonstrate that soot samples from different sources may have different active sites.

If the heterogeneous reaction of soot with O_3 is the diffusion controlled process, reactivities of soot samples with different microstructure should not show difference under the same reaction conditions. Different sites in the one soot sam-

ple also exhibit different reactivities to O_3, further determining that reaction of soot with O_3 is not the diffusion controlled process. Additionally, the uptake coefficient of O_3 on different soot also showed highly variable when diffusion of gas phase molecules has been taken into account in previous literatures.[21–25] Therefore, the difference in microstructure of different soot samples should be the essence of reason why uptake of O_3 on soot exhibits the variation. The reaction of soot with O_3 can be simply described by Eq. (1),

$$SS + O_3 \rightarrow Products. \tag{1}$$
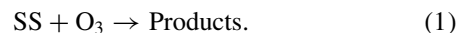
The kinetics expression of reaction (1) is given by Eq. (2),

$$\frac{d[SS]}{dt} = -k_{O_3} \times [O_3] \times [SS], \tag{2}$$

where k_{O_3} is the second order rate constant of the reaction. Under our experimental conditions, O_3 is a continuous flow through reactor. Thus, we can assume a pseudo-first-order reaction (Eq. (3)),

$$\frac{d[SS]}{[SS]} = -k_{obs} \times dt, \tag{3}$$

where $k_{obs} = k_{O_3} \times [O_3]$ is the experimental pseudo-first-order rate coefficient, [SS] can be replaced by integrated area of bands in Raman spectra if the integrated area is directly proportional to the surface concentration. As shown in Fig. 8, the areas of the disordered carbon at the graphene layer edges (*D1*) and surface graphene layers (*D2*) showed an exponential decrease pattern with ozonation time. This suggests that the reactions are reasonably described by pseudo-first-order kinetics. *D1* and *D2* were not completely consumed and reached a plateau after reaction with O_3 for 240 min. It means that some of *D1* and *D2* which were not accessible to O_3 and therefore did not participate in the reaction have not been
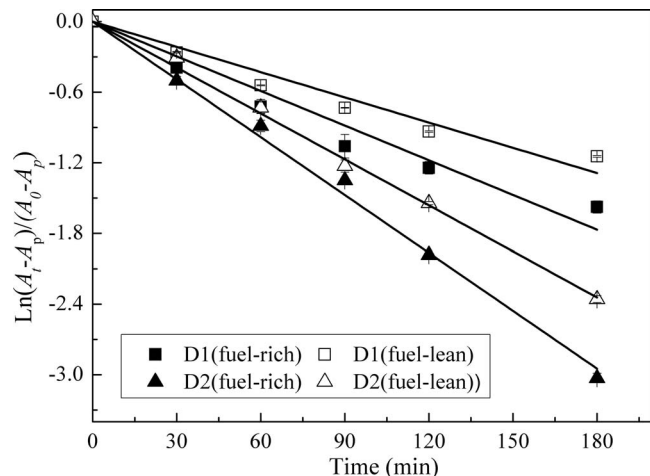
FIG. 9. Kinetics of *D1* (the disordered carbon at the graphene layer edges) and *D2* (the disordered carbon at surface graphene layers) bands for the "fuel-rich" and "fuel-lean" flame soot during reaction with 80 ppm O_3 at 298 K under atmospheric pressure.

considered in the determination of the reaction rate constant.[38–40] Therefore, the experimental data were fitted using pseudo-first order exponential functions shown in following equation:

$$\ln((A_t - A_p)/(A_0 - A_p)) = -kt, \qquad (4)$$

where t is the reaction time, A_0 and A_t are the integrated area percentages at the reaction time 0 and t min, respectively, and A_p is the peak area at the plateau after reaction for 240 min. k' represents the rate constant.

Figure 9 displays the kinetics of the *D1* and *D2* bands of the two types of soot samples during reaction with O_3. The k' of the *D1* and *D2* bands for the "fuel-rich" flame soot were $(9.82 \pm 0.58) \times 10^{-3}$ min^{-1} and $(1.64 \pm 0.03) \times 10^{-2}$ min^{-1}, respectively, and for the "fuel-lean" flame soot were $(7.15 \pm 0.41) \times 10^{-3}$ min^{-1} and $(1.30 \pm 0.02) \times 10^{-2}$ min^{-1}, respectively, which were lower by 37.3% and 26.2%. Correlation coefficients of these four bands were larger than 0.98, further suggesting that it is reasonable to assume a pseudo-first-order reaction. For the "fuel-rich" and "fuel-lean" flame soot, we found that the disordered carbon at the surface graphene layers (*D2*) more easily reacted with O_3 than that at graphene layer edges (*D1*). This means that different micro domains have different reactivity even within one sample. On the other hand, the k' values of the *D1* and *D2* bands for the "fuel-rich" flame soot were greater than that for the "fuel-lean" flame soot. This means that although they possessed the same reactive sites, these two samples had different reactivities to O_3 even when a given kind of site was considered. Additionally, the k' of 1750 cm^{-1} band for "fuel-rich" flame soot was also larger than that for "fuel-lean" flame soot (Fig. S4 of the supplementary material[41]). This result indicates that formation rate of the ketone, lactone, and anhydride species on "fuel-rich" flame soot is faster than that on "fuel-lean" flame soot. Generally speaking, one functional group in the different samples should have similar reactivity under the same conditions. The Raman band of a soot sample, however, only represents the vibration mode of a class of simi-

lar structures. For example, although the *D1* band represented the A_{1g} symmetry mode of the disordered graphitic lattice at graphene layer edges,[4] it is difficult to discriminate the imperceptible difference in Raman spectra among fragments with different size, on which the similar site might have different potential surface to O_3. Therefore, the differences in the reactivity of the *D1* (the disordered carbon at the graphene layer edges) and *D2* (the disordered carbon at surface graphene layers) band in these two soot samples might be related to the different micro-chemical structures formed under different combustion conditions. These results also suggest that the fragmental size at surface graphene layers and graphene layer edges of "fuel-rich" flame soot might be smaller than that of "fuel-lean" flame soot.

IV. CONCLUSIONS

Soot samples with different micro-chemical structure were produced by *n*-hexane combustion under different fuel/oxygen ratios. The diameter of the soot particles decreased from (29.8 ± 8.1) nm to (23.4 ± 7.6) nm as fuel/oxygen ratio decreased from 0.193 to 0.109. The FWHMs of the *D1* (the disordered carbon at the graphene layer edges), *D2* (the disordered carbon at surface graphene layers), *D3* (amorphous carbon), and *G* (the ideal graphitic lattice) bands increased obviously, while the FWHM of the *D4* (the disordered graphitic lattice or polyene-like structures) band shows a pronounced decrease as the fuel/oxygen ratio decreased. The relative contents of the *D1*, *D2*, and *D3* bands increased, while those of *D4* and *G* decreased as the fuel/oxygen ratio decreased from 0.193 to 0.109. These results indicate that combustion conditions not only affected the disorder degree for given microstructures, but also had a significant influence on the relative abundance of these microstructures in soot samples.

For "fuel-rich" flame soot, ozonization led to an increase in the FWHMs for all first-order Raman bands, while only three bands (*D1*, *D4*, and 1750 cm^{-1}) showed an increase in the FWHMs for the "fuel-lean" flame soot. For both the "fuel-rich" and "fuel-lean" flame soot, the integrated areas of the *D1* and *D2* bands showed a significant decrease, which implies the disordered carbon at the graphene layer edges and surface graphene layers were the reactive component for the heterogeneous reaction with O_3 and these two types of soot had the same active component for ozonization.

The apparent rate constant of the *D1* (the disordered carbon at the graphene layer edges) and *D2* (the disordered carbon at surface graphene layers) band to O_3 for the "fuel-rich" flame soot were $(9.82 \pm 0.58) \times 10^{-3}$ min^{-1} and $(1.64 \pm 0.03) \times 10^{-2}$ min^{-1}, respectively, and for the "fuel-lean" flame soot were $(7.15 \pm 0.41) \times 10^{-3}$ min^{-1} and $(1.30 \pm 0.02) \times 10^{-2}$ min^{-1}, respectively. The kinetics study demonstrated that the disordered carbon at surface graphene layers was more active than the disordered carbon at the graphene layer edges in one sample, and the reactivity of the disordered carbon at the graphene layer edges and surface graphene layers to O_3 in the "fuel-rich" flame soot was higher than that in the "fuel-lean" flame soot. These results highlight

the important role of the micro-chemical structures of soot in heterogeneous reactivity.

ACKNOWLEDGMENTS

[1] W. L. Chameides and M. Bergin, Science **297**, 2214 (2002).

[2] S. Menon, J. Hansen, L. Nazarenko, and Y. F. Luo, Science **297**, 2250 (2002).

[3] A. Sydbom, A. Blomberg, S. Parnia, N. Stenfors, T. Sandström, and S.-E. Dahlén, Eur. Respir. J. **17**, 733 (2001).

[4] Y. C. Liu, C. Liu, J. Z. Ma, Q. X. Ma, and H. He, Phys. Chem. Chem. Phys. **12**, 10896 (2010).

[5] V. Zelenay, M. E. Monge, B. D'Anna, C. George, S. A. Styler, T. Huthwelker, and M. Ammann, J. Geophys. Res. **116**, D11301, doi:10.1029/2010JD015500 (2011).

[6] M. E. Monge, B. D'Anna, L. Mazri, A. Giroir-Fendler, M. Ammann, D. J. Donaldson, and C. George, Proc. Natl. Acad. Sci. U.S.A. **107**(15), 6605 (2010).

[7] D. G. Aubin and J. P. D. Abbatt, J. Phys. Chem. A **111**, 6263 (2007).

[8] A. F. Khalizov, M. Cruz-Quinones, and R. Y. Zhang, J. Phys. Chem. A **114**, 7516 (2010).

[9] J. Kleffmann and P. Wiesen, Atmos. Chem. Phys. **5**, 77 (2005).

[10] J. Kleffmann, K. H. Becker, M. Lackhoff, and P. Wiesen, Phys. Chem. Chem. Phys. **1**, 5443 (1999).

[11] S. Lelièvre, Y. Bedjanian, G. Laverdet, and G. L. Bras, J. Phys. Chem. A **108**, 10807 (2004).

[12] S. Lelièvre, Y. Bedjanian, N. Pouvesle, J.-L. Delfau, C. Vovelle, and G. L. Bras, Phys. Chem. Chem. Phys. **6**, 1181 (2004).

[13] H. M. Daly and A. B. Horn, Phys. Chem. Chem. Phys. **11**, 1069 (2009).

[14] H. X. Xue, A. F. Khalizov, L. Wang, J. Zheng, and R. Y. Zhang, Phys. Chem. Chem. Phys. **11**, 7869 (2009).

[15] F. Arens, L. Gutzwiller, U. Baltensperger, H. W. Gaggeler, and M. Ammann, Environ. Sci. Technol. **35**, 2191 (2001).

[16] D. Zhang and R. Y. Zhang, Environ. Sci. Technol. **39**, 5722 (2005).

[17] G. Hantal, S. Picaud, P. N. M. Hoang, V. P. Voloshin, N. N. Medvedev, and P. Jedlovszky, J. Chem. Phys. **133**, 144702 (2010).

[18] F. Moulin, S. Picaud, and P. N. M. Hoang, J. Chem. Phys. **127**, 164719 (2007).

[19] A. Striolo, A. A. Chialvo, K. E. Gubbins, and P. T. Cummings, J. Chem. Phys. **122**, 234712 (2005).

[20] H. A. Al-Abadleh and V. H. Grassian, J. Phys. Chem. A **104**, 11926 (2000).

[21] J. McCabe and J. P. D. Abbatt, J. Phys. Chem. C **113**, 2120 (2009).

[22] S. Kamm, O. Möhler, K.-H. Naumann, H. Saathoff, and U. Schurath, Atmos. Environ. **33**, 4651 (1999).

[23] A. R. Chughtai, J. M. Kim, and D. M. Smith, J. Atmos. Chem. **45**, 231 (2003).

[24] U. Poschl, T. Letzel, C. Schauer, and R. Niessner, J. Phys. Chem. A **105**, 4029 (2001).

[25] R. S. Disselkamp, M. A. Carpenter, J. P. Cowin, C. M. Berkowitz, E. G. Chapman, R. A. Zaveri, and N. S. Laulainen, J. Geophys. Res. **105**, 9767, doi:10.1029/1999JD901189 (2000).

[26] A. M. Nienow and J. T. Roberts, Annu. Rev. Phys. Chem. **57**, 105 (2006).

[27] B. Dippel, H. Jander, and J. Heintzenberg, Phys. Chem. Chem. Phys. **1**, 4707 (1999).

[28] A. Sadezky, H. Muckenhuber, H. Grothe, R. Niessner, and U. Pöschl, Carbon **43**, 1731 (2005).

[29] S.-K. Sze, N. Siddique, J. J. Sloan, and R. Escribano, Atmos. Environ. **35**, 561 (2001).

[30] H. Muckenhuber and H. Grothe, Carbon **44**, 546 (2006).

[31] N. Ivleva, A. Messerer, X. Yang, R. Niessner, and U. Pöschl, Environ. Sci. Technol. **41**, 3702 (2007).

[32] E. Weingartner, H. Burtscher, and U. Baltensperger, Atmos. Environ. **31**(15), 2311 (1997).

[33] C. Alcala-Jornod and M. J. Rossi, J. Phys. Chem. A **108**, 10667 (2004).

[34] C. Han, Y. C Liu, C. Liu, J. Z. Ma, and H. He, J. Phys. Chem. A **116**, 4129 (2012).

[35] W. Choi and M.-T. Leu, J. Phys. Chem. A **102**, 7618 (1998).

[36] D. M. Smith and A. R. Chughtai, J. Atmos. Chem. **26**, 77 (1997).

[37] T. Gruber, T. W. Zerda, and M. Gerspacher, Carbon **32**(7), 1377 (1994).

[38] J. Z. Ma, Y. C Liu, and H. He, Atmos. Environ. **45**, 917 (2011).

[39] J. Z. Ma, Y. C Liu, and H. He, Atmos. Environ. **44**, 4446 (2010).

[40] E. Perraudin, H. Budzinski, and E. Villenave, J. Atmos. Chem. **56**, 57 (2007).

[41] See supplementary material at http://dx.doi.org/10.1063/1.4747190 for curve fitting results of Raman spectra for the ozonised fuel-rich flame soot and kinetics of 1750 cm^{-1} band during reaction.